Growth valley dividing single- and multi-walled carbon nanotubes: combinatorial study of nominal thickness of Co catalyst

Kazunori Kakehi[1], Suguru Noda[1*], Shigeo Maruyama[2], and Yukio Yamaguchi[1]

[1] Department of Chemical System Engineering, School of Engineering, The University of Tokyo, 7-3-1 Hongo, Bunkyo-ku, Tokyo 113-8656, Japan

[2] Department of Mechanical Engineering, School of Engineering, The University of Tokyo, 7-3-1 Hongo, Bunkyo-ku, Tokyo 113-8656, Japan

The relationship among the nominal thickness of Co catalyst, the structure of the catalyst particles, and the structure of carbon nanotubes (CNTs) growing from the catalysts was investigated. A gradient thickness profile of Co was prepared by a combinatorial method and then subjected to alcohol catalytic chemical vapor deposition at 700 ˚C. In the deposited sample, two active regions appeared on either side of an inactive region. In the active regions, mainly single-walled carbon nanotubes (SWNTs) or multi-walled carbon nanotubes (MWNTs) grew depending on the nominal Co thickness (SWNTs at about 0.1 nm Co thickness, and MWNTs at about 1.5 nm). However, neither SWNTs nor MWNTs grew efficiently at a moderate Co thickness (~ 0.4 nm). This dependence of CNT growth on the initial Co thickness is explained by the different mechanisms for catalyst particle formation from a sub-nanometer-thick Co film and from a nanometer-thick Co films.

KEYWORDS: single-walled carbon nanotubes, multi-walled carbon nanotubes, chemical vapor deposition, catalytic growth mechanism, nanoparticle formation, ethanol, combinatorial method

* Corresponding author. E-mail address: noda@chemsys.t.u-tokyo.ac.jp

1. Introduction

Single-walled carbon nanotubes (SWNTs) are a nanomaterial that has attracted much attention for their application in nanodevices due to their unique properties,[1] such as metallic or semiconductive conductivity depending on chirality, high mechanical strength, and large specific surface area, etc. SWNTs have been extensively researched, and they can now be grown either by physical vapor deposition and by chemical vapor deposition (CVD). Various methods, such as "HiPco",[2] "CoMoCAT",[3] "alcohol catalytic CVD (ACCVD)",[4] "SuperGrowth",[5] and "e-DIPS",[6] have been developed for CVD, all of which utilize metal nanoparticles as catalysts. In these catalytic CVD methods, carbon-source molecules adsorb on the nanoparticles, and then, carbon atoms dissolve into the nanoparticles and precipitate to form SWNTs.[7, 8] The size of the nanoparticles are generally believed to determine the diameter and the number of walls of the carbon nanotubes (CNTs).[7-9] Relationship between diameter of nanoparticles and SWNTs has been investigated for floating[10] or substrate-supported[11-16] catalysts experimentally and calculated by molecular dynamics simulation,[17] in all of which the diameter of SWNTs was slightly smaller than that of particles. In the case of catalyst deposited by sputtering, Yamada, et al. reported that the diameter and the number of walls of CNTs growing from C_2H_4 was controlled by the nominal thickness of the initial Fe catalyst layer,[18] presumably because the thicker initial Fe layer yielded larger Fe particles. Reaction conditions during CVD can also affect the diameter of the CNTs. Lu, et al. reported that the diameter of SWNTs grown by the same catalyst of polydisperse Fe nanoparticles increased with increasing partial pressure of C_2H_6.[19] In this way, SWNT growth is largely dependent on both the catalyst conditions (e.g., catalyst type and particle size) and reaction conditions (e.g., carbon-source type, temperature, and

pressure). In addition, effects of these conditions interact with each other in a complex manner. Fundamental understanding of the growth mechanism of SWNTs is still important for both basic and application aspects.

To study the catalyst conditions systematically, we previously developed a combinatorial method,[20] in which a gradient thickness profile of a catalyst is prepared on a substrate and transformed into a series of catalyst particles of various sizes and areal densities at the elevated CVD temperature. This method enables the systematic investigation of catalyst conditions even in a single CVD run. By using this method, we found that the optimum thicknesses of Co[21] and Ni[22] catalysts on SiO_2 are as thin as 0.1 and 0.2 nm, respectively, for the SWNT growth by ACCVD.[5]

In this study, the range of catalyst Co thickness was expanded to thicker region (from 0.06 to 3.8 nm) than that of the previous study (0.036 to 0.27 nm),[21] and the relationship among the nominal thickness of a catalyst (Co), structure of the particles, and structure of CNTs was investigated in detail. As a result, growth valley dividing SWNTs and multi-walled carbon nanotubes (MWNTs) was observed. And the underlying mechanisms of both spontaneous formation of nanoparticles and catalytic growth of CNTs were discussed.

2. Experiment

Gradient thickness profiles of Co were prepared on Si substrates with a thermal oxide layer or on quartz glass substrates. These substrates were pretreated with mixed solution of H_2SO_4 aq. (95 wt.%) and H_2O_2 aq. (30 wt.%) whose ratio was 3:1 in volume, and then washed with de-ionized water. Catalysts were deposited on these substrates by sputtering with a mask. The mask was a 0.5-mm thick metal sheet with a 2-mm wide slit

and placed 3.6 mm above the substrate.[23] Co was deposited at 1.3 Pa through the slit-mask by r.f. magnetron sputtering system with 4 inch targets. Gradient thickness profile of Co was obtained perpendicular to the slit with the nominal Co thickness (t_{Co}) ranging from 0.06 to 3.8 nm. The samples with uniform Co thickness were also prepared without the mask. The samples were exposed to air and then placed in a hot-wall quartz-glass tubular reactor. The samples were heated to 700 ˚C under 5 vol% H_2/Ar flow at 2.7 kPa, kept at this temperature for 10 min, and then ACCVD was carried out by introducing pure ethanol vapor into the reactor at 1.3 kPa for 10 min. Some samples were annealed at 700 ˚C under 5 vol% H_2/Ar atmosphere for 10 min without ACCVD to observe Co particles just before ACCVD. The resulting samples were characterized by micro-Raman scattering spectroscopy (Seki Technotron, STR-250) with an excitation wavelength at 488 nm and field emission scanning electron microscopy (FE-SEM, Hitachi, S-4700 and S-900). Further observation was made by transmission electron microscopy (TEM, JEOL, 2000EX and 2010F). As-grown CNTs were transferred from the substrate to TEM grids by just rubbing the substrate surfaces with the grids. For TEM observation of Co particles on the substrate just before ACCVD, specimen preparation was carried out by ion milling method. The substrates were mechanically thinned, dimpled by dimple grinder (Gatan, 656) and polished by Precision Ion Polishing System (Gatan, S-691) operated at Ar^+ acceleration voltage of 3-5 keV.

3. Results and Discussion

Figure 1(a) shows an optically scanned image of the substrate after ACCVD for 10 min by a commercially available film scanner and Fig. 1(b) shows average

absorbance of visible light by the substrate estimated from Fig. 1(a). The nominal thickness profile of Co ranged from 0.05 nm (at left on the sample) to 3.8 nm (right) as shown in Fig. 1(c). Five regions at around 1, 5, 9, 12, and 14 mm from the left edge of the substrate were named as Regions I, II, III, IV, and V, respectively. Regions II, IV, and V (t_{Co} = 0.13, 1.5, 3.8 nm, respectively) showed dark color and Region V was colored mainly due to a nominally 2-4-nm-thick Co.

Figure 2(a) shows the Raman spectra of the CNTs grown for Regions I-V. The peak area ratio of G-band to D-band increased with decreasing t_{Co}. For Region II, this ratio was 15.2, which is about three times larger than that for Region IV. CNTs grown at Region II had higher crystalline quality than those at Region IV. Figure 2(b) shows the G-band peak area in Raman spectra as a function of t_{Co}. The amount of graphitic material can be roughly estimated from the G-band area although the intensity of G-band depends on the quality or crystallinity of the graphitic material. The peak area was higher for Regions II and IV than for the other regions. Comparing these two regions, the G-band peak at Region II was half that at Region IV, although in the optically scanned image (Fig. 1) Region II was much lighter than Region IV. The optimum t_{Co} for SWNT growth was 0.1 nm in our previous study,[21] which is approximately the same t_{Co} of Region II (0.13 nm) in this study. The other region, i.e. Region IV, was newly found in this study because this region was not studied in the previous work.[21]

Figure 3 shows TEM images of as-grown CNTs at the two active Regions II and IV. SWNTs mainly grew at Region II, and most of them formed bundles. The diameters of the SWNTs themselves ranged from about 1.5 to 2.5 nm. There is a deviation in estimated diameters between TEM and Raman (Fig. 2a); the main RBM

peak at 200 cm^{-1} originates from SWNTs with a diameter of 1.2 nm. The sensitivity of RBM decreases as the diameter of SWNTs increases, and therefore, a small amount of thin SWNTs contained in thicker SWNTs possibly yielded the RBM peak at 200 cm^{-1}. Diameter of 1.5-2.5 nm by TEM is more reliable than that of 1.2 nm by Raman. In contrast, MWNTs mainly grew at Region IV, and a few SWNTs were evident. In this region, the diameters of the MWNTs ranged from about 10 to 15 nm and had walls that were bent and gnarled, indicating low quality MWNTs.

Figure 4 shows FE-SEM images used to further study the microstructure of CNTs as-grown on the substrate. Plan-view FE-SEM images show sparse CNTs (presumably individual SWNTs) for Region I, a network of CNTs (SWNT bundles) for Region II, sparse CNTs for Region III, a dense network of CNT bundles for Region IV, and thick, hollow tubes for Region V. Qualitatively, all three evaluation methods (optical transparency in Fig. 1, Raman spectra in Fig. 2, and FE-SEM images in Fig. 4) revealed the same tendency in CNT amount against t_{Co}, namely, with increasing t_{Co}, the amount first increased, decreased, increased, and again decreased.

Figure 5 shows a plan-view TEM image of catalyst particles after annealing at 700 ˚C under 5 vol% H_2/Ar atmosphere without ACCVD. Note that this image reflects the particle structure just before CVD but not during CVD; incorporation of carbon into catalyst particles during CVD may cause further structural change. The particles for Regions II and IV were observed at t_{Co} = 0.13 and 1.5 nm, respectively, but the obtained images were not clear at t_{Co} = 0.13 nm. At t_{Co} = 1.5 (Region IV), the particle diameter distribution was bimodal with a respective average of 4.6 ± 1.1 nm and 20 - 30 nm. Because the number of larger particles in TEM was too small, we counted several tens of the larger particles by SEM (Fig. 6(b) IV) and obtained their average diameter as 15

nm. This average diameter was similar to that of MWNTs (insets of IV in Fig. 3), and therefore, these larger particles were likely catalysts for MWNTs.

The structure of Co particles were further clarified by preparing uniform Co films with t_{Co} = 0.06, 0.13, 0.43, 1.5, and 3.8 nm on separate substrates, then annealing at 700 ˚C under 5 vol% H_2/Ar atmosphere, and finally observing them by FE-SEM. At $t_{Co} \geq 0.13$ nm (Regions II-V), Co particles were not observed before annealing (Figs. 6(a)), but after annealing (Figs. 6(b)), particles were observed; small diameter particles (about 5 nm or less) at a high areal density of around 10^{12} /cm^2 in the background, and large diameter particles (10-30 nm) at a lower areal density below 1×10^{11} /cm^2. Especially, a drastic change was observed between Region II and Region III in the areal density of the large particles from 0.67×10^{10} /cm^2 (Region II) to 5.2, 6.8, 4.7×10^{10} /cm^2 (Regions III, IV, V, respectively). These large particles increased their size with increasing t_{Co}. Whereas the structural change of the small particles was not clarified by SEM.

The mechanisms for Co particle formation should differ, depending on Co layer thickness t_{Co}. For thin initial Co layers ($t_{Co} \leq 0.13$ nm), the submonolayer-thick Co cannot form a continuous layer and thus particle formation possibly proceeded via surface diffusion of Co adatoms, resulting in small Co particles with a unimodal size distribution. In contrast, for thick initial Co layers ($t_{Co} \geq 0.43$ nm), the layer was thick enough to form a continuous layer partly. In addition to the formation of small particles via surface diffusion of adatoms, elastic deformation of the layer driven by surface tension possibly occurred simultaneously, resulting in the formation of large particles. It should be noted that bimodal distribution can appear even within SWNTs; nominally 0.8-nm-thick Co (between Regions III and IV) grew SWNTs with a bimodal diameter of

1-2 and 3-4 nm at 750 °C and 4.0 kPa, possibly because the higher temperature and ethanol pressure caused Ostwald ripening among small particles of a-few-nm-diameters, resulted into a bimodal diameter distribution. Details will be presented in a separate work.[24)]

Figure 7 schematically illustrates the possible mechanisms for the above-mentioned results. Before annealing (Fig. 7(a)), Co has different structures depending on t_{Co}; particles at $t_{Co} \leq 0.13$ nm (Regions I and II) and semi-continuous layers at 0.43 nm $\leq t_{Co}$ (Regions III, IV, and IV). After annealing (Fig. 7(b)), particles are formed depending on the initial structure of Co; small particles by diffusion (Regions I and II) and large particles by surface tension in addition to the small particles (Region III, IV, and V). The diameter of the smaller particles formed by surface diffusion depends on t_{Co}; the diameter increases with increasing t_{Co}. The same trend is true for large particles formed by surface tension; the diameter increases with increasing t_{Co}. The formation of the large particles may make the small particles smaller because most catalyst form large particles and only the residual catalyst forms small particles. Actually, SWNTs grown at Region IV appears somewhat thinner than those grown at Region II because they show RBM peaks at larger wavenumbers for Region IV than for Region II as can be seen in Fig. 2(a). Apparently, at Region IV, small particles had suitable diameters for growing SWNTs and large particles had suitable diameters for growing MWNTs. At Region III, small particles might be too small for growing SWNTs and large particles might be too small for growing MWNTs. The hypothesis described above on the particle formation by two mechanisms can explain the existence of the growth valley. We are now carrying out further investigation to obtain experimental evidences and studying the underlying mechanism for the dependence of the catalytic

activity of SWNT/MWNT growth on the catalyst particle size.

4. Conclusions

The relationship among the nominal thickness of the initial catalyst layer, the structure of the particles spontaneously formed from that layer, and the structure of carbon nanotubes (CNTs) grown from those particles was investigated for ACCVD with Co/SiO_2 catalysts. Experimental results of Raman spectra, SEM and TEM images, as well as optical absorbance revealed two optimum thicknesses: sub-nanometer thickness (0.13 nm) for the formation of SWNTs and nanometer thickness (1.5 nm) for the formation of MWNTs (MWNTs accompanied some SWNTs). A catalyst layer between these two optimal thicknesses yielded limited CNT growth. Smaller Co particles (about 5 nm or less) with unimodal size distribution were formed from a sub-nanometer-thick Co layer, whereas Co particles with a bimodal size distribution (i.e., smaller particles and larger particles, 3-6, ≥ 10 nm, respectively) were formed from a nanometer-thick Co layer. These results reveal different mechanisms for spontaneous formation of these smaller particles and larger particles, and reveal optimum sizes for these particles to efficiently grow SWNTs and MWNTs.

Acknowledgements

The authors thank Mr. H. Tsunakawa, Mr. K. Ibe, and Mr. T. Ito for assistance in the TEM observations, and Ms. Z. Zhang for assistance in the Raman measurements. This work was financially supported in part by a Grant-in-Aid for Young Scientists (A), 18686062, 2006, from the Ministry of Education, Culture, Sports, Science and Technology (MEXT), Japan.

References

1) R. Saito, G. Dresselhaus, and M. S. Dresselhaus: *Physical Properties of Carbon Nanotubes* (Imperial College Press, London, 1998).

2) P. Nikolaev, M. J. Bronikowski, R. K. Bradley, F. Rohmund, D. T. Colbert, K. A. Smith, and R. E. Smalley: Chem. Phys. Lett. **313** (1999) 91.

3) J. E. Herrera, L. Balzano, A. Borgna, W. E. Alvarez, and D. E. Resasco: J. Catal. **204** (2001) 129.

4) S. Maruyama, R. Kojima, Y. Miyauchi, S. Chiashi, and M. Kohno: Chem. Phys. Lett. **360** (2002) 229.

5) K. Hata, D. N. Futaba, K. Mizuno, T. Namai, M. Yumura, and S. Iijima: Science **306** (2004) 1362.

6) T. Saito, W. Xu, S. Ohshima, H. Ago, M. Yumura, and S. Iijima: J. Phys. Chem. B **110** (2006) 5849.

7) H. Dai, A. G. Rinzler, P. Nikolaev, A. Thess, D. T. Colbert, and R. E. Smalley: Chem. Phys. Lett. **260** (1996) 471.

8) J. Liu, S. Fan, and H. Dai: Mater. Res. Bull. **29** (2004) 244.

9) A. Oberlin, M. Endo, and T. Koyama: J. Cryst. Growth **32** (1976) 335.

10) A. G. Nasibulin, P. V. Pikhitsa, H. Jiang, and E. I. Kauppinen: Carbon **43** (2005) 2251.

11) C. L. Cheung, A. Kurtz, H. Park, and C. M. Lieber: J. Phys. Chem. B **106** (2002) 2429.

12) G. H. Jeong, S. Suzuki, Y. Kobayashi, A. Yamazaki, H. Yoshimura, and Y. Homma: J. Appl. Phys. **98** (2005) 124311.

13) G. H. Jeong, A. Yamazaki, S. Suzuki, Y. Kobayashi, and Y. Homma: Chem. Phys.

Lett. **422** (2006) 83.

14) G. H. Jeong, A. Yamazaki, S. Suzuki, Y. Kobayashi, H. Yoshimura, and Y. Homma: Carbon **45** (2007) 978.

15) G. H. Jeong, S. Suzuki, Y. Kobayashi, A. Yamazaki, H. Yoshimura, and Y. Homma: Appl. Phys. Lett. **90** (2007) 043108.

16) M. Ishida, H. Hongo, F. Nihey, and Y. Ochiai: Jpn. J. Appl. Phys. **43** (2004) L1356.

17) Y. Shibuta and S. Maruyama: Chem. Phys. Lett. **382** (2003) 381.

18) T. Yamada, T. Namai, K. Hata, D. N. Futaba, K. Mizuno, J. Fan, M. Yudasaka, M. Yumura, and S. Iijima: Nat. Nanotechnol. **1** (2006) 131.

19) C. Lu and J. Liu: J. Phys. Chem. B **110** (2006) 20254.

20) S. Noda, Y. Kajikawa, and H. Komiyama: Appl. Surf. Sci. **225** (2004) 372.

21) S. Noda, Y. Tsuji, Y. Murakami, and S. Maruyama: Appl. Phys. Lett. **86** (2005) 173106.

22) K. Kakehi, S. Noda, S. Chiashi, and S. Maruyama: Chem. Phys. Lett. **428** (2006) 381.

23) S. Noda, H. Sugime, T. Osawa, Y. Tsuji, S. Chiashi, Y. Murakami, and S. Maruyama: Carbon **44** (2006) 1414.

24) H. Sugime, S. Noda, S. Maruyama, and Y. Yamaguchi: to be submitted.

Figure captions

Fig. 1 (a) Optically scanned image of the substrate after ACCVD at 700 ˚C for 10 min by a commercially available film scanner. (b) Average absorbance of visible light by the substrate estimated from (a). (c) Nominal Co thickness (t_{Co}) profile. t_{Co} ranged from 0.06 nm (at left on the substrate) to 3.8 nm (right).

Fig. 2 (a) Raman spectra of carbon nanotubes measured using 488-nm excitation. Intensity at the low wavenumber region (< 350 cm^{-1}) is shown magnified by a factor 10 in this figure. (b) Peak area of G-band of Raman spectra as a function of t_{Co}.

Fig. 3 TEM images of CNTs as-grown on a substrate with uniform initial Co layers of thickness t_{Co} = 0.13 and t_{Co} = 1.0 nm (corresponding to Regions II and IV, respectively). Insets show individual CNTs, and scale bars are 10 nm.

Fig. 4 Plan-view FE-SEM images of as-grown CNTs with initial Co layers of thickness t_{Co} = 0.06, 0.13, 0.43, 1.5, and 3.8 nm (Regions I-V, respectively).

Fig. 5 A plan-view TEM image of Co particles with a uniform initial Co layer of thickness t_{Co} = 1.5 nm (Region IV).

Fig. 6 Plan-view FE-SEM images (a) before and (b) after annealing under H_2/Ar atmosphere at uniform initial Co layer thickness t_{Co} = 0.06, 0.13, 0.43, 1.5, 3.8 nm (Regions I-V, respectively). Scale bars in insets are 50 nm. The objects at the bottom-left corner of Regions I-V in (a) and Region I in (b) are dust particles used for

focus adjustment.

Fig. 7 Schematic models of spontaneous formation of Co particles (a) before and (b) during H_2/Ar annealing, and that of (c) CNT growth during ACCVD for Regions I-V.

Fig. 1

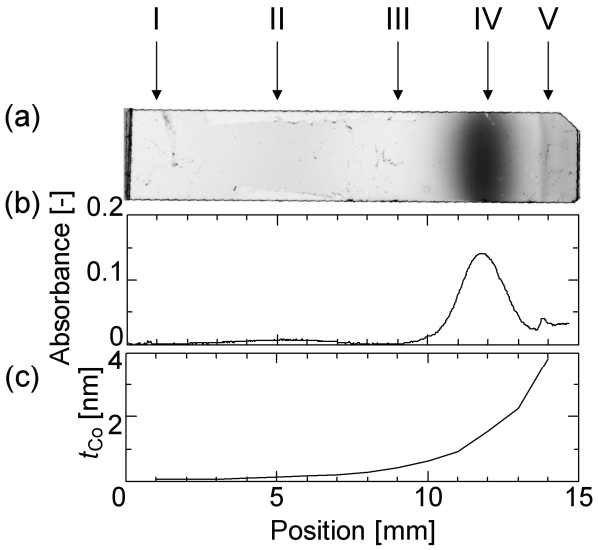
I
II
III
IV
V
(a)
(b)
Absorbance [-]
0.2
0.1
0
(c)
t_{Co} [nm]
4
2
0
5
10
15
Position [mm]

Fig. 2

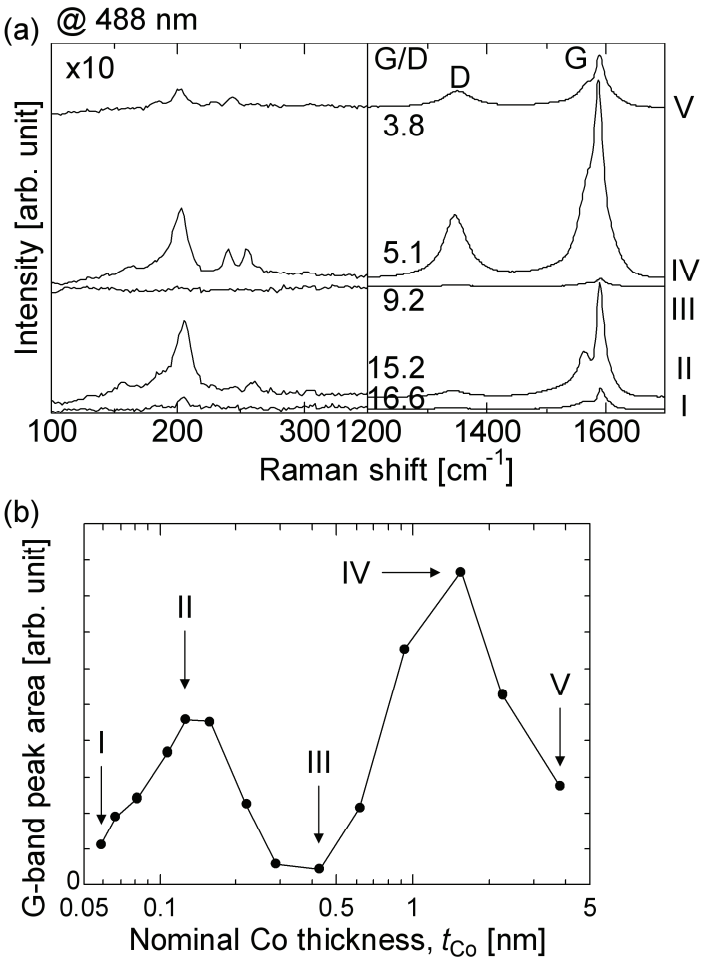
(a)
@ 488 nm
x10
G/D
D
G
V
3.8
5.1
IV
9.2
III
15.2
II
16.6
I
Intensity [arb. unit]
100
200
300
1200
1400
1600
Raman shift [cm-1]
(b)
G-band peak area [arb. unit]
IV
II
V
I
III
0
0.05
0.1
0.5
1
5
Nominal Co thickness, tCo [nm]

Fig. 3

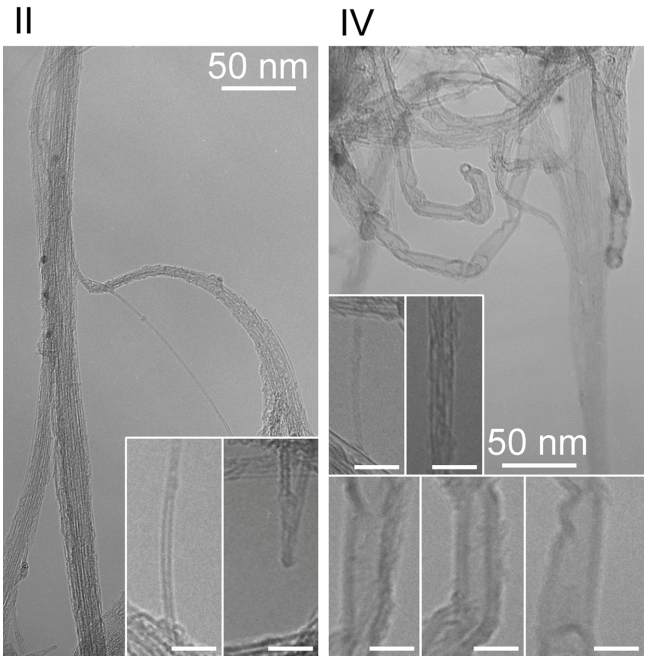

Fig. 4

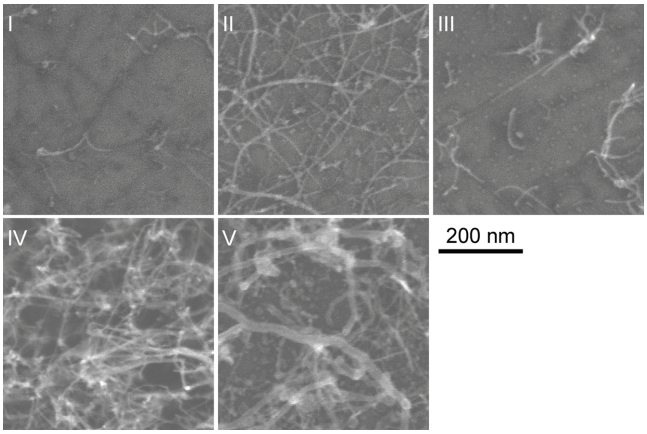

Fig. 5

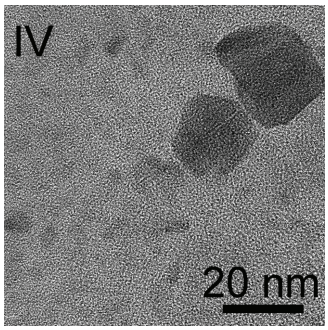

Fig. 6

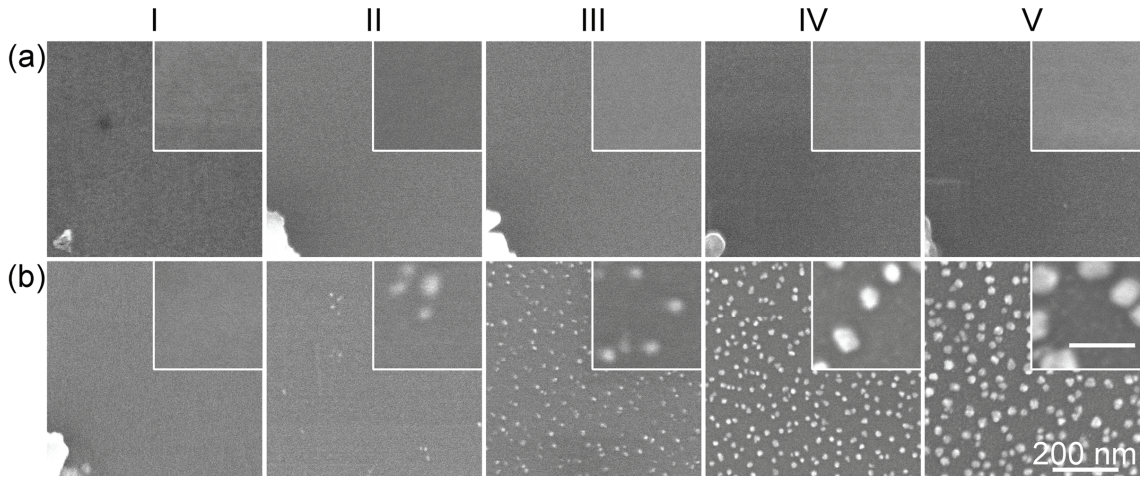

Fig. 7